*Article*

# Photovoltaic-Battery-Ultracapacitor-Diesel Hybrid Generation System for Mobile Hospital Energy Supply

**Mohamed Zine Zizoui [1]**, **Muhammad Fahad Zia [2]**, **Bekheira Tabbache [1]**, **Yassine Amirat [3,*]**, **Abdeslam Mamoune [4]** and **Mohamed Benbouzid [4,5]**

[1] UER ELT, Ecole Militaire Polytechnique, Alger 16111, Algeria; zimozine.1975@gmail.com (M.Z.Z.); laid_tabache@yahoo.com (B.T.)

[2] Department of Electrical Engineering, National University of Computer and Emerging Sciences, Lahore 54000, Pakistan; fahad.zia@nu.edu.pk

[3] L@bISEN, ISEN Yncréa Ouest, 29238 Brest, France

[4] Institut de Recherche Dupuy de Lôme (UMR CNRS 60 27 IRDL), University of Brest, 29238 Brest, France; Abdeslam.Mamoune@univ-brest.fr (A.M.); Mohamed.Benbouzid@univ-brest.fr (M.B.)

[5] Logistics Engineering College, Shanghai Maritime University, Shanghai 201306, China

\* Correspondence: yassine.amirat@isen-ouest.yncrea.fr

**Abstract:** This paper deals with the energy management of a hybrid power system, which consists of a photovoltaic (PV) system, diesel generators, battery, and ultracapacitor for a mobile hospital. The proposed power system can supply energy to shelter hospitals for better treatment of patients in remote states, particularly in the event of a pandemic situation such as Coronavirus Disease 2019 (COVID-19). For this reason, a hybrid power system in which a diesel generator is used with a photovoltaic energy source for reliable availability of power supply. Moreover, battery and ultracapacitor are also integrated to obtain a hybrid power generation and storage system to ensure the smooth operation of mobile hospitals irrespective of weather conditions. A boost converter is used with PV panels to operate them in either maximum power tracking mode or power curtailment mode. The battery is connected to a bidirectional reversible DC-DC converter for direct-current (DC) bus voltage regulation and state of charge control. The ultracapacitor is associated with the battery to compensate for the peak power. The diesel generator is connected in parallel with the photovoltaic generator, battery, and ultracapacitor to continuously provide the power required by the load. The integrated operation of all generation sources and storage systems is complex for shelter hospitals. Therefore, an efficient energy management algorithm is developed to manage the continuous energy flow between different elements of the hybrid power system and mobile hospital load through the control of the power converters. Finally, validation results are presented to show the effectiveness of the proposed energy management algorithm for the hybrid power system.

**Keywords:** photovoltaic generator; battery; ultracapacitor; diesel generator; energy management; mobile hospital

## 1. Introduction

In remote areas and particularly in the sub-Saharan territories, the low population distribution causes difficulties in ensuring on-site health coverage in emergency cases requiring medical evacuation, such as the Coronavirus Disease 2019 (COVID-19) pandemic [1,2]. Therefore, mobile hospitals are needed to be built or deployed in the desert and remote areas. These hospitals include different medical treatment and diagnostic equipment, which are essentially required in medical emergency [3]. The smooth operation of these medical devices requires a continuous power supply from diesel generators, which result in high fuel costs and preventive maintenance [4,5].

In remote areas with high solar potential, the combination of a diesel generator (DG) with photovoltaic (PV) generators offers better energy services in terms of reduced oper-

ating costs and achievement of gradual transition from fossil to renewable sources [6,7]. In case of low demand, excess energy from PV generators needs to be stored using energy storage systems. However, some medical devices may require high peak power, and batteries suffer from a short life span due to suddenly high energy requirements (5–10 years) and low dynamic behavior [8]. However, peak power demand can be supported by ultracapacitors due to their high power density capability [9,10]. The management of all these generation sources and storage systems presents a major challenge in determining the relationship between energy production and consumption in a mobile hospital. In this context, there are few research studies in the literature that address this problem [11]. The profile of electrical energy consumption is illustrated in an isolated hotel where its consumption is pre-determined according to the number of clients or visits during the year [12]. On the other hand, the authors in [13] have proposed a model for distributing the energy produced between different departments of a hospital while minimizing the energy cost. In the same context, the resiliency of a hospital is studied in [14] by optimizing the sizing of its generation sources. The hospital is powered by renewable energy and a conventional generation source. The techno-economic potential of hybrid power generation systems is studied for refugee camps and rural areas [15,16]. Nonetheless, all these studies do not consider a mobile hospital, which is needed in the case of medical emergencies.

For medical emergencies, the reliability of a hybrid power generation system for mobile hospitals is also important. In this regard, the mean time between failure (MTBF) of different generators, converters, and wirings plays a vital role in determining reliability for continuous energy supply to critical applications like mobile hospitals [17]. In case of DG failure, the main backup source has been lost for mobile hospitals. Hence, MTBF of DG must be incorporated at the planning and sizing stages of hybrid power generation systems for mobile hospitals [18,19]. Moreover, an inverter source can also be added as a redundant power supply on each floor to ensure a reliable power supply for mobile hospitals.

The integration of different production and storage systems for mobile hospitals requires an efficient energy management strategy. Many papers have proposed microgrid applications that are designed for autonomous operation, where the main control objective is to know how to manage the energy flow between the different loads of the system. In the microgrid framework, various control strategies have been proposed in the literature. A frequency-based power-sharing method is presented in [20] to mitigate the effect of weather or sea state variations on the integrated onboard ship microgrid. A hybrid energy storage system (HESS) based on ultracapacitor and battery is developed such that high power and short-term fluctuations are handled by the battery and ultracapacitor. Proportional integral derivative (PID) and proportional derivative (PD) based control methods are introduced in [21] for the smooth operation of hybrid power generation under steady-state and dynamic operating conditions, respectively. In [22], the power balance control is achieved for a multi-source microgrid hybrid system to meet the DC load power demand while ensuring DC bus voltage stabilization. In the same context, Ref. [23] proposes a coupling structure of the DG on the DC bus side to slow down the power dynamics produced by the DG and ensure the efficiency and profitability of the system by operating the DG around its rated power. A voltage and frequency control strategy is developed in [24] for a renewable power generation system. An inverter interfaced energy storage system is connected with an AC bus instead of a conventional generator to regulate system frequency.

Most of the energy management techniques presented above require the DG to remain operational most of the time for avoiding transition regimes of operating modes. In [25,26], a transition control strategy between the connected and disconnected modes of the grid was proposed for a three-phase voltage source based on the calculation of reference powers and a virtual impedance control strategy to achieve efficient power distribution in the hybrid energy storage elements, where the battery provides steady-state power and supports only transient power fluctuations.

This paper proposes a new energy flow supervision for a PV-diesel-HESS microgrid that efficiently manages the operation of generation and storage systems in different

operating modes. For PV system management, it is connected with a boost converter to operate in either maximum power tracking mode or power curtailment (Off-MPPT) mode. The battery is connected to a bidirectional DC-DC converter, which regulates the DC bus voltage and controls the state of charge (SOC) of the battery. The ultracapacitor is also included with the batteries to compensate for peak power demand. The diesel generator is connected in parallel with the PV generator, battery, and ultracapacitor to provide the insufficient power required by the load. For the efficient operation of all these generation sources and storage systems, an energy management algorithm is developed to manage the energy flow between the sources and load through effective control of power converters.

## 2. Power Sizing of Mobile Hospital

Table 1 presents a list of medical and non-medical equipment with their estimated daily energy needs according to their power consumption priority. In hybrid power system designing, the proper sizing of each source is important. It must be efficiently determined such that the continuous power supply is ensured for smooth energy availability at a lower cost. The sizing depends on both the location-dependent meteorological characteristics and the required load demand. A typical daily load profile of a mobile hospital is shown in Figure 1.

The hybrid power system is presented in Figure 2. It is composed of a photovoltaic generator as a renewable energy source, battery, ultracapacitor, diesel generator as a source of emergency energy, and power electronics converters as elements of electric power exchange of energy flow in the system. PV generator is connected with a boost converter. However, the battery and ultracapacitor are connected to bidirectional DC-DC converters. The diesel generator is connected in parallel with the DC bus through a bidirectional inverter while it is directly connected with the AC load.

During the design, the sizing of the power appears as an important aspect. It must be done in such a way as to ensure a continuous power supply while ensuring energy availability at a lower cost. The sizing depends on both the meteorological characteristics depending on the location and the required load demand. However, this paper focuses only on proposing energy management and control structure for the hybrid power system of a mobile hospital.
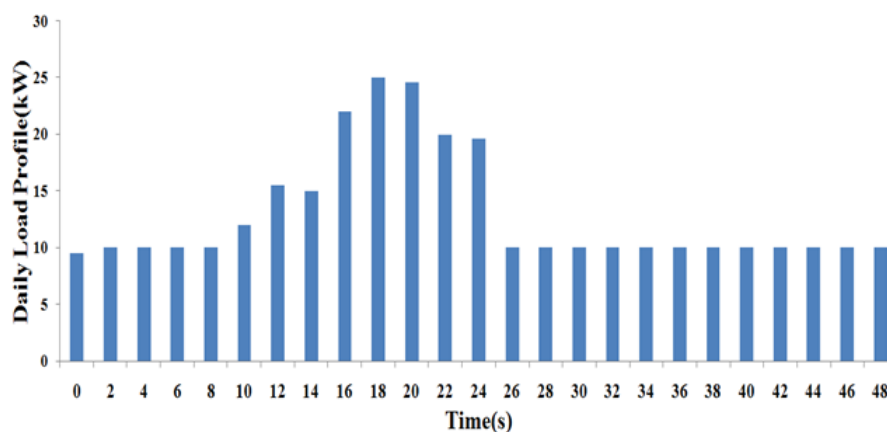


**Figure 1.** Typical load profile of a mobile hospital.

**Table 1.** Electricity consumption devices in a mobile hospital.

| Basic Equipment | | | | | | |
| --- | --- | --- | --- | --- | --- | --- |
| Equipment | Power (W) | Hours Used per Day (h) | Energy per Day (Wh/Day) | First Priority | Second Priority | Third Priority |
| Lights (fluorescent) | 11 | 8 | 88 | x | | |
| Mobile phone charger | 5–20 | 8 | 40–160 | | | x |
| Ceiling fan (DC, AC) | 30–100 | 8 | 300–800 | | | x |
| Water pump | 100 | 6 | 600 | x | | |
| Computer | 15–200 | 4.5 | 67.5–900 | | x | |
| Portable electrical heater | 1000–1500 | 2 | 2000–3000 | | | x |
| Radio | 2–30 | 8 | 16–240 | | | x |
| Printer (ink, laser) | 65–1000 | 2 | 130–2000 | | x | |
| Small waste autoclave | 600–6000 | 1 | 600–6000 | | | x |
| **Medical Equipment** | | | | | | |
| Sterilizer (steam) | 500–1560 | 2 | 1000–3200 | | | x |
| Suction | 24 | 10 | 240 | | x | |
| Pulse Oximetry | 24 | 3 | 72 | x | | |
| Reverse-osmosis Water purifier | 260-570 | 7 | 1820–2590 | x | | |
| X-ray machine (dental) | 200 | 1 | 200 | x | | |
| X-ray machine (portable and fixed) | 300–2000 | 2 | 600–4000 | x | | |
| Mechanical ventilator | 608 | 3 | 1824 | | x | |
| Ultrasound scanner | 75 | 2–3 | 150–225 | x | | |
| Electrocardiogram (ECG) | 50–80 | 1 | 50–80 | | x | |
| Nebulizer | 180 | 3–5 | 540–900 | | | x |
| **Laboratory Equipment** | | | | | | |
| Vaccine refrigerator (165 L) | 40–500 | 4 | 160–2000 | x | | |
| Microscopes | 30 | 2 | 60 | | x | |
| Centrifuge | 600 | 1.5 | 900 | | x | |
| Spectrophotometer | 63 | 1 | 63 | | | |
| Blood chemistry analyzer | 45 | 2 | 90 | x | | |
| Hematology Analyzer | 230 | 2 | 460 | | x | |
| Arterial blood gas (ABG) analyzer | 250 | 0.5 | 125 | x | | |
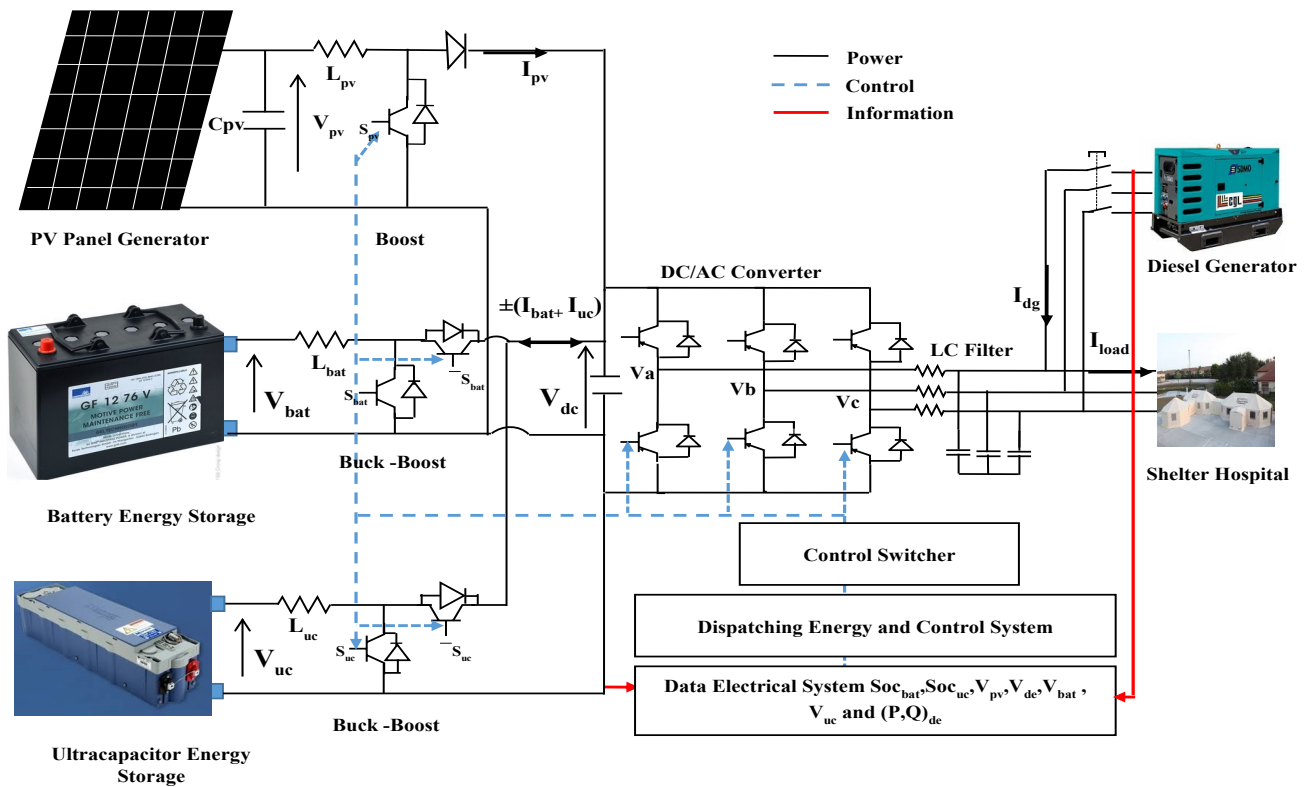
**Figure 2.** Parallel hybrid power generation system structure for a mobile hospital.

## 3. Hybrid System Structure

### 3.1. PV Generator

PV cells are made of pure Silicon with other added chemical elements to enhance their efficiency [27,28]. PV cells are normally connected in either parallel or series connections to create PV modules of operating voltage suitable for electrical applications. PV modules are used to absorb solar energy for converting into DC electrical energy, which can be either directly fed to loads or stored in battery [29,30]. Hence, the desired electric power rating of the PV module can be obtained using the required number of PV cells. The PV cell can be modeled in an equivalent electrical circuit, which is shown in Figure 3 [31,32]. Using Kirchhoff's law, the PV current is determined as:

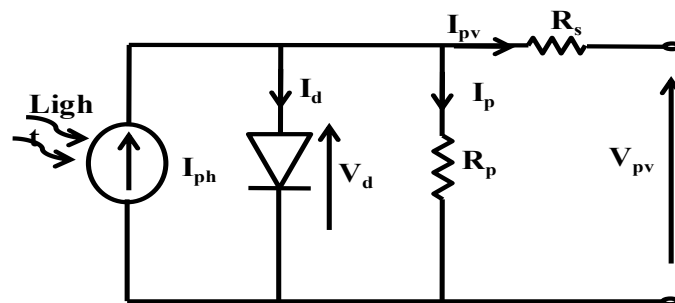$$I_{pv} = I_{ph} - I_d - I_p \tag{1}$$



**Figure 3.** Electric circuit model of PV cell.

The characteristic equation of current and voltage is provided by Equation (2) for a PV module with $N_s$ PV cells connected in series and $N_p$ PV cells connected in parallel.

$$I_{PV} = N_p I_{ph} - N_p I_0 \left( e^{\left( \frac{V_{PV} + R_{sG} I}{N_s a V_T} \right)} - 1 \right) - \frac{V_{PV} + R_{sG} I_{PV}}{R_{pG}} \tag{2}$$

where $R_{sG} = \frac{N_s R_s}{N_p}$ and $R_{pG} = \frac{N_s R_p}{N_p}$. $I_{pv}$ and $V_{pv}$ are current (A) and voltage (V) of a PV module, respectively. $I_{ph}$ is the photo current (A) and $I_O$ is saturation current. $R_{sG}$ and $R_{pG}$ are resistances ($\Omega$) of series and parallel cells, respectively.

### 3.2. Battery

Different equivalent electric models for battery exist in the literature [32–35]. In this paper, the equivalent electrical model of battery is presented in Figure 4. The battery model consists of an ideal battery as a voltage source $E_o$, an internal leakage resistance $R_{bat}$, polarization resistance $R_p$, and polarization capacitance $C_p$ [34,35]. The output voltage of battery is modeled as:

$$V_{bat} = E_0 - (R_{bat} \times I_{bat}) - V c_p,$$
$$\dot{V} c_p = -\frac{1}{R_p C_p} V c_p + \frac{1}{C_p} I_{bat}. \tag{3}$$

The battery SOC is determined using the following relationship:

$$SOC_{bat} = \left( SOC_0 - \int_0^t \frac{Q_d}{Q_{bat}} \, dt \right) \times 100\% \tag{4}$$

where $SOC_{bat}$ and $SOC_0$ are the actual and initial SOCs of the battery in ($Ah$), respectively. $Q_d$ is its used quantity of charge and $Q_{bat}$ is its total capacity.
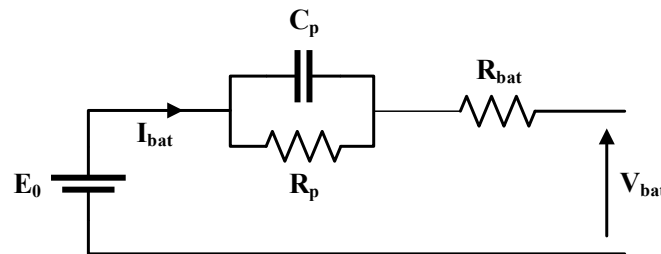


**Figure 4.** Electric model of battery.

### 3.3. Ultracapacitor

The equivalent electrical model of ultracapacitor, as shown in Figure 5, is composed of equivalent serial resistance ($R_{es}$), equivalent parallel resistance ($R_{ep}$), and capacitor ($C_{uc}$) [36,37]. The SOC of ultracapacitor is expressed as a function of the voltage at the terminals of the ultracapacitors using the following relation:

$$SOC_{uc} = \frac{V_{uc}}{V_{nom-uc}} \tag{5}$$

where $V_{nom-uc}$ is the load nominal voltage.
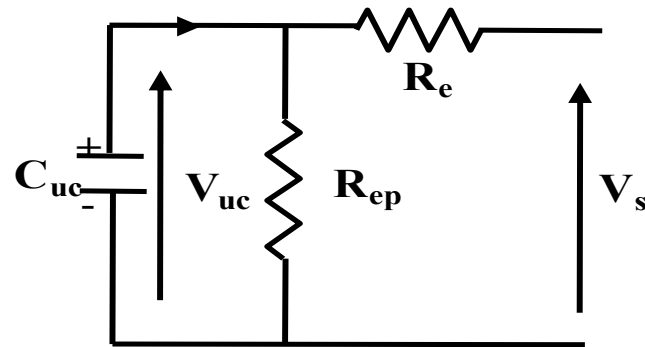
**Figure 5.** Electric model of ultracapacitor.

### 3.4. Diesel Generator

Diesel generator is composed of a diesel engine, a synchronous generator, and the excitation system as shown in Figure 6 [38,39]. The control of a diesel engine governor is illustrated in Figure 7. The DG torque model is given as,

$$T_{mec} = \varphi(s)e^{(-s\tau_1)} \tag{6}$$

$$\frac{d\Omega}{dt} = \frac{1}{J_T}(T_{mec} - T_e - D_T\Omega) \tag{7}$$

$$\varphi(s) = \frac{ka}{(1 + s\tau_2)}C \tag{8}$$
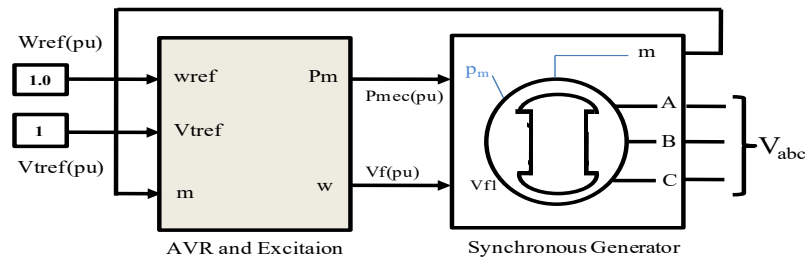
where $\varphi(s)$ is the fuel flow.



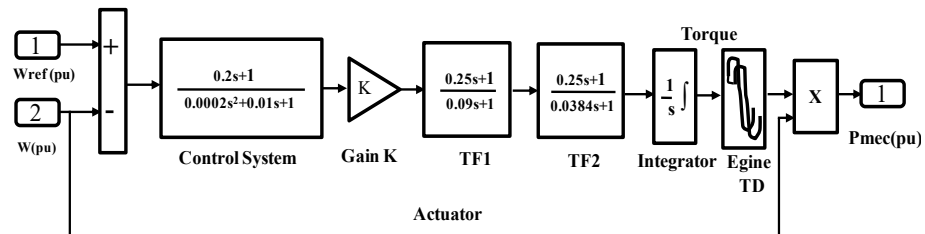**Figure 6.** Schematic diagram of a diesel generator.



**Figure 7.** Schematic diagram of diesel engine governor.

## 4. Power Management of Hybrid System

### 4.1. PV Generator Control

PV generator is connected to the DC bus through a boost converter as shown in Figure 8. The boost converter is used to operate the PV generator in MPPT or off-MPPT modes. The MPPT of PV generator is achieved using Perturb and Observe algorithm which is presented in Figure 9a. The control algorithm for power curtailment of PV generator

is illustrated by Figure 9b. The DC-DC boost converter can be modeled by the following relationship:

$$\begin{cases} \frac{di_L}{dt} = \frac{1}{L}\left(V_{pv} - (1+d)V_{dc}\right) \\ \frac{dV_{pv}}{dt} = \frac{1}{C_{pv}}\left(i_{pv} - i_L\right) \end{cases} \tag{9}$$

In terms of MPPT, the Perturb and Observe (P&O) method is widely adopted due to its effectiveness and simplest implementation [40–42]. This method only requires voltage and current measurements of PV generators to extract maximum power from it. With perturbation in the input voltage, the power output of the PV generator is observed to determine the next control action for the boost converter. This process continues until maximum power is extracted from PV generator.

If electrical power increases, the perturbation should continue in the same direction. Otherwise, the perturbation direction will be inverse.
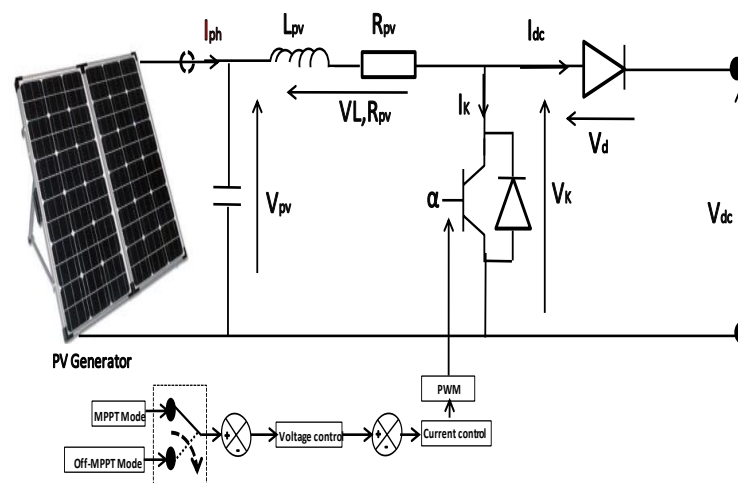


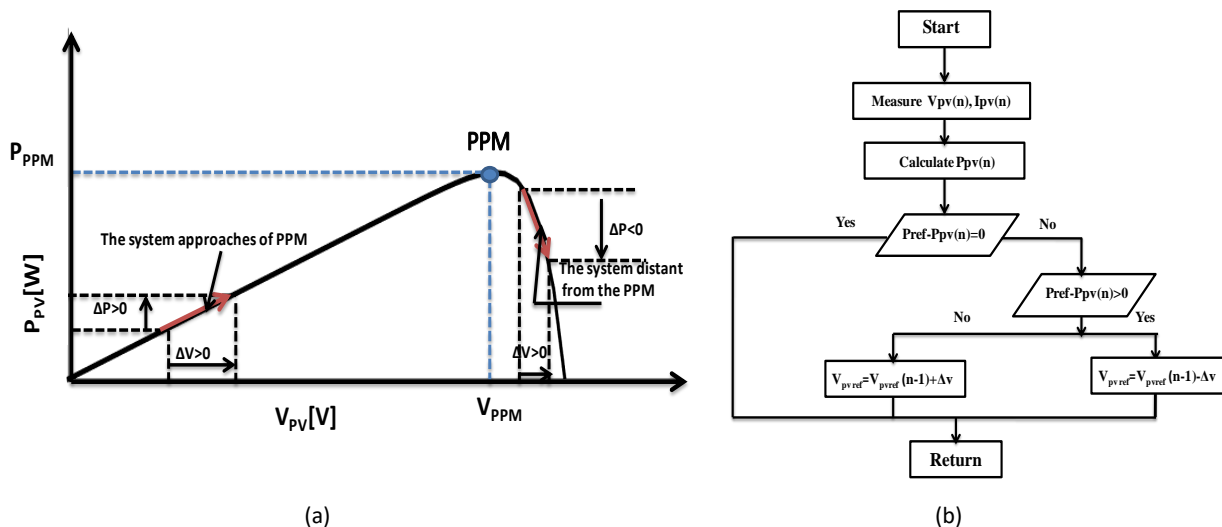**Figure 8.** Boost converter for PV generator with both control modes.



(a)

(b)

**Figure 9.** (**a**) Perturb and Observe-based MPPT, (**b**) Off-MPPT mode (power curtailment).

### 4.2. DC Bus Control

Figure 10 shows that the battery and ultracapacitor are connected to bidirectional DC-DC converters. A frequency separation controller is used for efficient power management between battery and ultracapacitor storage systems. Both of these energy storage systems

have two operating modes; charging and discharging. The bidirectional DC-DC converter of the battery can be modeled by:

$$\frac{di_{bat}}{dt} = \frac{1}{L}\left(\alpha_{bat}V_{dc} - V_{bat}\right) \tag{10}$$

Bidirectional DC-DC converter of the ultracapacitor can be modeled by:

$$\frac{di_{uc}}{dt} = \frac{1}{L}\left(\alpha_{uc}V_{dc} - V_{uc}\right) \tag{11}$$

To regulate the DC bus voltage by the frequency separation technique, the storage elements should provide currents equal to the common current $I_L$.
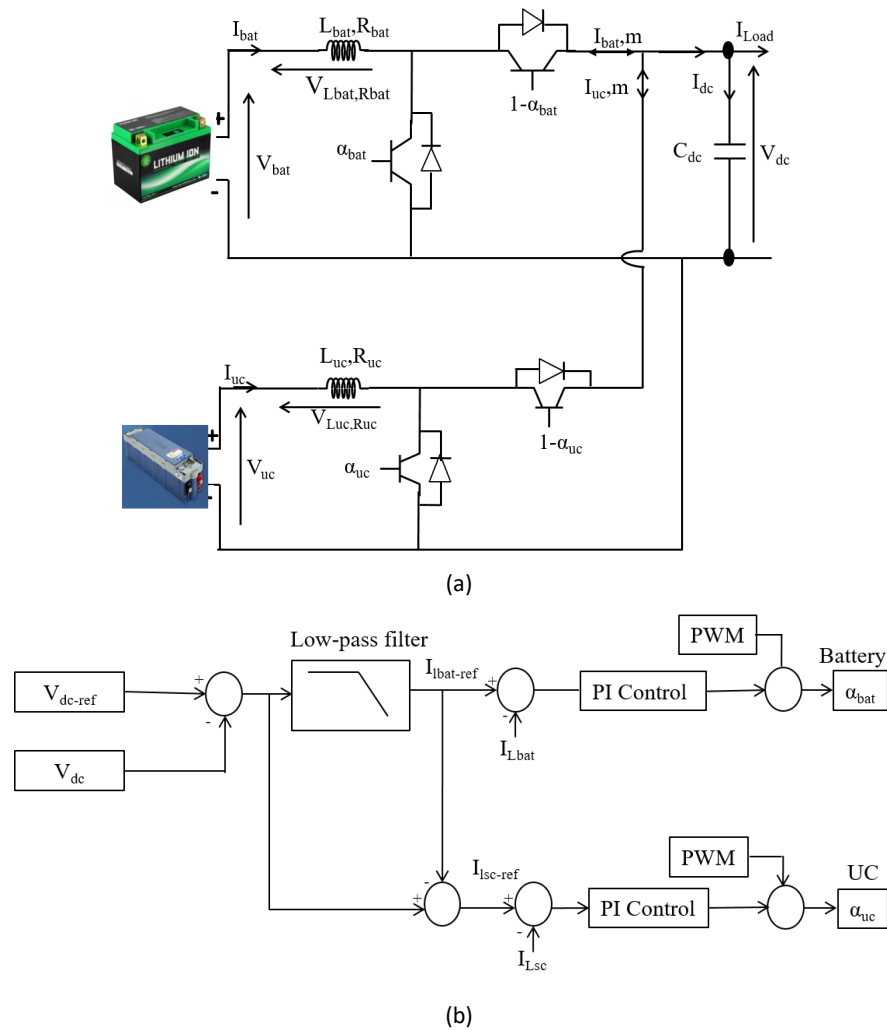


(a)

(b)

**Figure 10.** (**a**) Bidirectional DC-DC converters for hybrid storage system, (**b**) Frequency separation scheme of hybrid storage system.

The DC bus voltage is coordinately controlled by the battery and ultracapacitor sources. The DC bus voltage Vdc is compared with the reference DC bus voltage $Vdc_{ref}$. The difference represents the input of the proportional-integration (PI) controller, which provides the current reference $I_{ref}$.

Figure 10b presents the concept of the frequency separation scheme. After the low-pass filter (LPF) of the current reference, the high-frequency component of the DC bus is passed to the ultracapacitor and the low-frequency component goes to the battery controller. In this way, the battery current reference ($I_{Lbat-ref}$) can be obtained and the reference current of

the ultracapacitor ($I_{Luc-ref}$) is obtained by the difference between the two currents ($I_{L-ref}$) and ($I_{Lbat-ref}$).

### 4.3. AC Bus Control

Two operating modes, grid-connected and off-grid, are explained in the following subsections.

#### 4.3.1. Grid-Disconnected Mode (Off-Grid)

In this mode, the DG is disconnected from the AC bus. The purpose of this mode is to control the inverter to provide a regulated AC voltage based on the dq-frame technique. For this, the voltage across the filter capacitor should be regulated for which the voltage reference contains nonzero frequencies. This method provides good control performance and protects against overloads and short circuits [43–45].

This type of technique is shown in Figure 11, where $L_f$, $R_f$, and $C_f$ represent the inductor, internal resistance of the inductor, and capacitor of the LC filter, respectively. $V_{dc}$ represents the regulated voltage. The regulated voltage across the capacitor is the voltage supplied to the three-phase load. The switching method is based on pulse width modulation. The differential equations describing the dynamics of the inverter are modeled as follows:

$$V_{inv,abc} = mV_{dc} = R_f I_{L,abc} + L_f \frac{dI_{L,abc}}{dt} + V_{abc} \tag{12}$$

$$I_{L,abc} = C_f \frac{dV_{abc}}{dt} + I_{Load,abc} \tag{13}$$

$$\begin{bmatrix} V_d \\ V_q \end{bmatrix} = \frac{1}{CS} \begin{bmatrix} (Cw)V_q \\ -(Cw)V_d)] \end{bmatrix} + \frac{1}{CS} \begin{bmatrix} I_{Ld} - I_{Load-d} \\ I_{Lq} - I_{Load-q} \end{bmatrix} \tag{14}$$

$$\begin{bmatrix} I_{Ld} \\ I_{Lq} \end{bmatrix} = \frac{1}{L_f S + R_f} \begin{bmatrix} V_{id} - V_d \\ V_{iq} - V_q \end{bmatrix} + \frac{1}{L_f S + R_f} \begin{bmatrix} (L_f w)I_{Lq} \\ -(L_f w)I_{Ld} \end{bmatrix} \tag{15}$$

where $V_{inv,abc}$ is three phase inverter output voltage, $m$ is the three-phase control signal, $V_{abc}$ is the three phase filter capacitor output voltage, and $I_{Load,abc}$ is the three phase load output current.
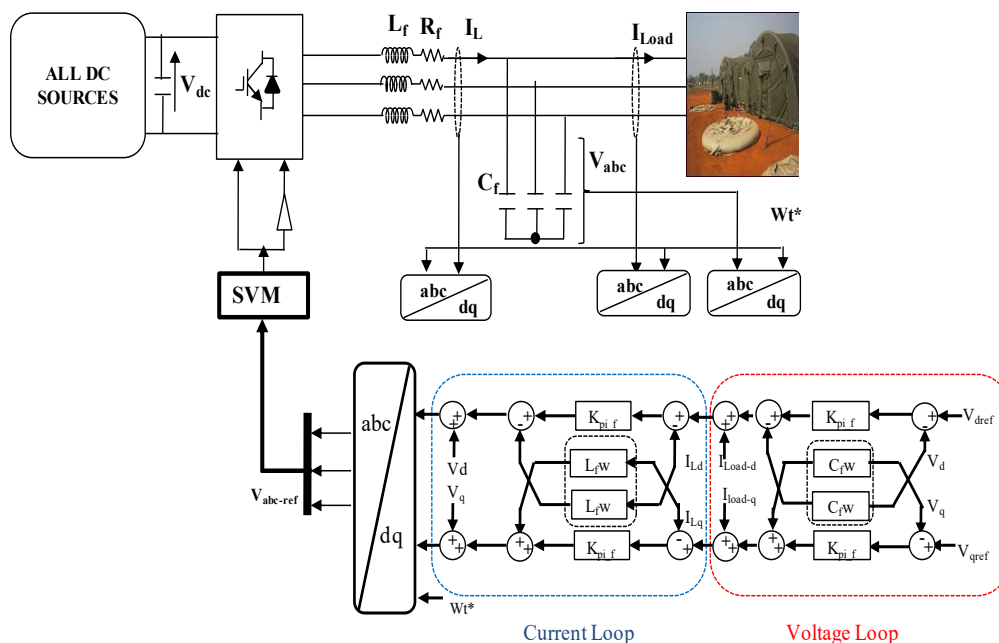


**Figure 11.** dq-frame control method for AC bus.

### 4.3.2. Grid-Connected Mode

In this mode, the diesel generator is connected to the AC bus and the DC bus voltage is connected to the AC bus via a bidirectional inverter with an LC filter. Thus, the diesel generator can operate in parallel with the inverter by synchronizing the output voltages. A phase-locked loop (PLL) is used to estimate the angular frequency of AC voltage in the control system.

The power inverter control is based on the voltage orientation control (VOC), which is illustrated in Figures 12 and 13. It uses the instantaneous powers (active and reactive) and the output voltage of the diesel generator [46,47]. The voltage across the LC-filter is given by:

$$V_{an} = L_f \frac{di_{Lf}}{dt} + R_f i_{Lf} + V_{cf} \tag{16}$$

In a diesel generator connected mode, the $V_{cf} = 0$

$$V_{an} + V_{DG,a} = L_f \frac{di_{Lf}}{dt} + R_f i_{Lf} \tag{17}$$

$$I_{Load,abc} = I_{DG,abc} + I_f \tag{18}$$

The conventional convergence of a mathematical model of a stationary coordinate system with the synchronous rotary two-phase coordinate system (dq) is presented according to the following equations:

$$\begin{cases} V_D = L_f \frac{dI_D}{dt} + R_f I_D - L_f w I_Q + E_D \\ V_Q = L_f \frac{dI_Q}{dt} + R_f I_Q + L_f w I_D + E_Q \end{cases} \tag{19}$$

$$\begin{cases} L_f \frac{dI_D}{dt} + R_f I_D = \left(K_p + \frac{K_i}{s}\right) \times (I_{d-ref} - I_D) \\ L_f \frac{dI_Q}{dt} + R_f I_Q = \left(K_p + \frac{K_i}{s}\right) \times (I_{q-ref} - I_Q) \end{cases} \tag{20}$$
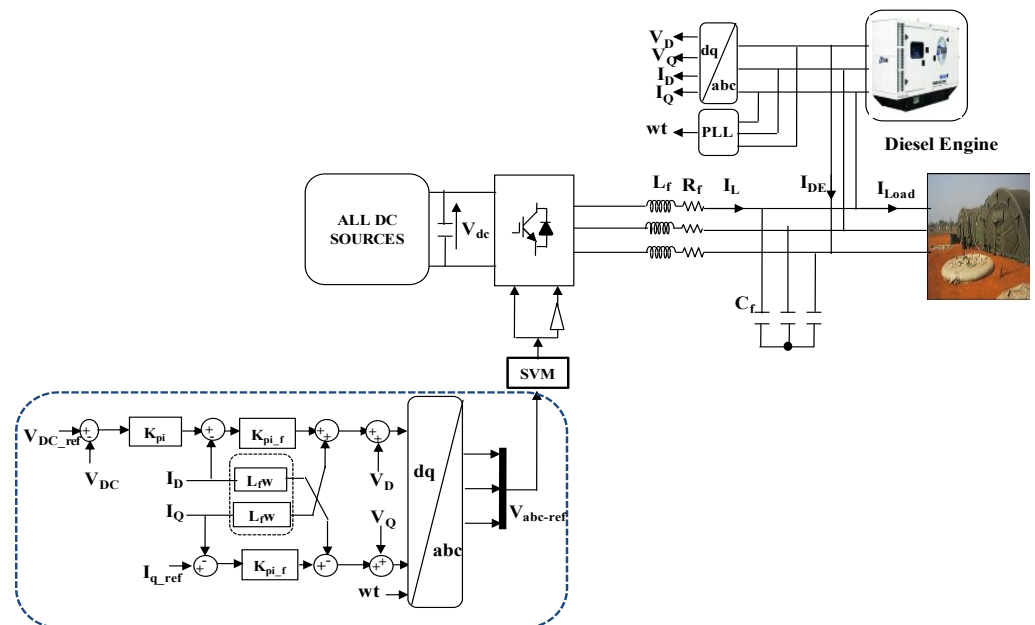


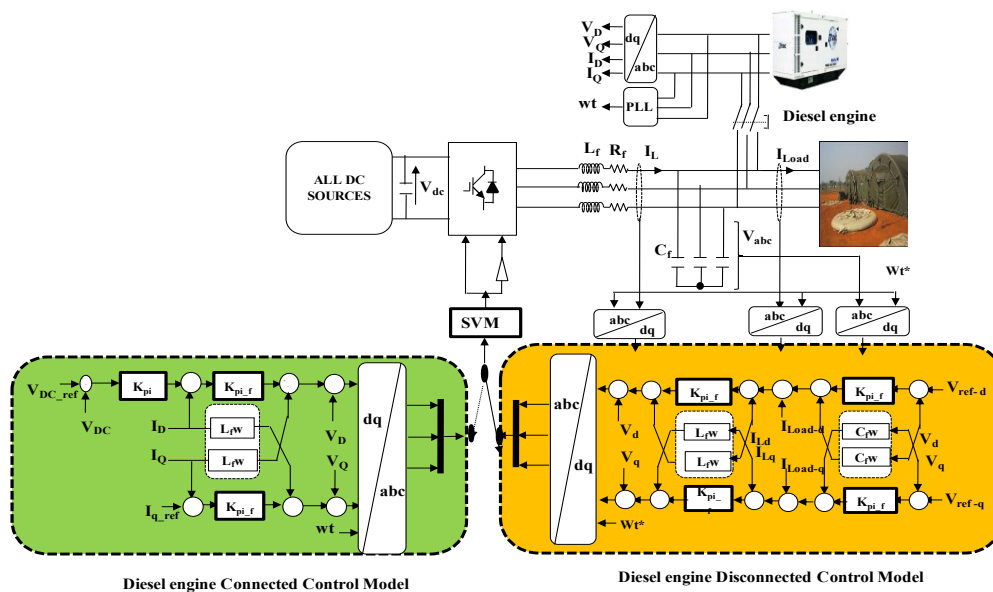**Figure 12.** Functional diagram of voltage-oriented control approach.

**Figure 13.** Inverter control approaches for both grid-connected and disconnected modes.

Using (19) and (20), the final expression is given by:

$$\begin{cases} V_{d-ref} = \left(K_p + \frac{K_i}{s}\right) \times (I_{d-ref} - I_D) - L_f w I_Q + E_D \\ V_{q-ref} = \left(K_p + \frac{K_i}{s}\right) \times (I_{q-ref} - I_Q) + L_f w I_D + E_Q \end{cases} \tag{21}$$

## 5. Power Management Strategy

Power management and sharing in the electrical system are developed according to the state of charge and discharge of the battery storage system. In this case, the ultracapacitor state of charge is kept between 97.4% and 98.4%. The proposed power management strategy of the battery is illustrated by Figure 14, while Figure 15 illustrates the ultracapacitor level balancing algorithm.

The proposed power management strategy contains seven operating modes as presented in Table 2.

**Table 2.** Power management operating modes.

| | | Different Operating Modes | | | | | | |
|---|---|---|---|---|---|---|---|---|
| Stage | State of Hybrid Storage (%) | PCM | MPPTM | DEDM | DECM | FPLM | SPLM | TPLM |
| 1 | $SOC_{bat} \geq 90\%$ | 1 | 0 | 1 | 0 | 1 | 1 | 1 |
| 2 | $25\% \leq SOC_{bat} < 90\%$ | 0 | 1 | 1 | 0 | 1 | 1 | 1 |
| 3 | $15\% \leq SOC_{bat} < 25\%$ | 0 | 1 | 0 | 1 | 1 | 1 | 0 |
| 4 | $10\% \leq SOC_{bat} < 15\%$ | 0 | 1 | 0 | 1 | 1 | 0 | 0 |
| 5 | $SOC_{bat} < 10\%$ | 0 | 1 | 0 | 1 | 0 | 0 | 0 |

Start

Check $SOC_{bat}$

$90\% > SOC_{bat} < 25\%$ — Yes / No

$SOC_{bat} > 90\%$ — Yes / No

PCM

$SOC_{bat} = 25\%$ — Yes / No

$SOC_{bat} = 90\%$ — Yes / No

$SOC_{bat} < 25\%$ — No / Yes

Check $SOC_{bat}$

MPPTM

DECM

$SOC_{bat} = 90\%$ — Yes / No

MPPTM

$SOC_{bat} < 25\%$ — Yes / No

TPLM

$SOC_{bat} < 15\%$ — Yes / No

SPLM

$SOC_{bat} < 10\%$ — Yes / No

FPLM
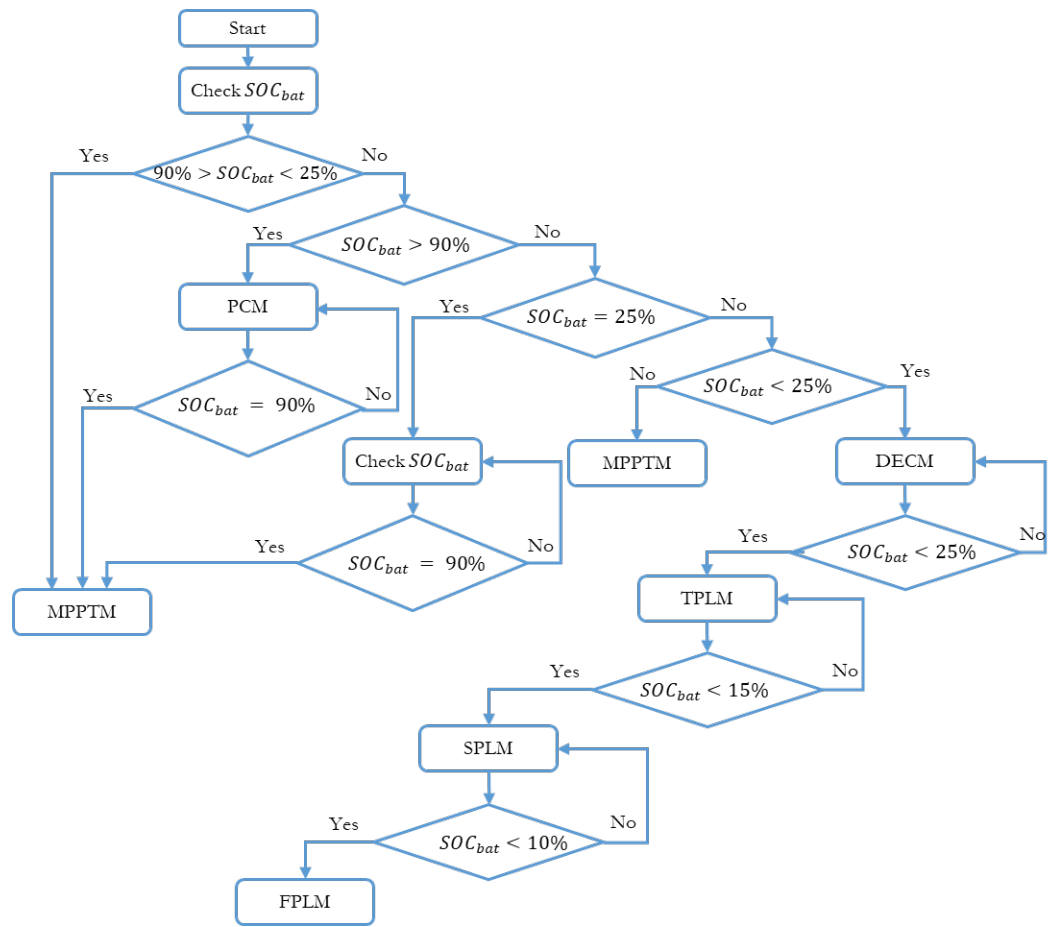
**Figure 14.** Power management flowchart for the battery storage system.

UC Balancing $SOC_{bat}$

$98.4\% > SOC_{UC} > 97.4\%$ — Yes / No

$SOC_{UC} > 98.4\%$ — Yes / No

$SOC_{UC} < 97.4\%$ — Yes / No

Baluc Mode = 0 & Puc = 0

Puc Bal Mode = 500W & The UC discharging until 98.4%

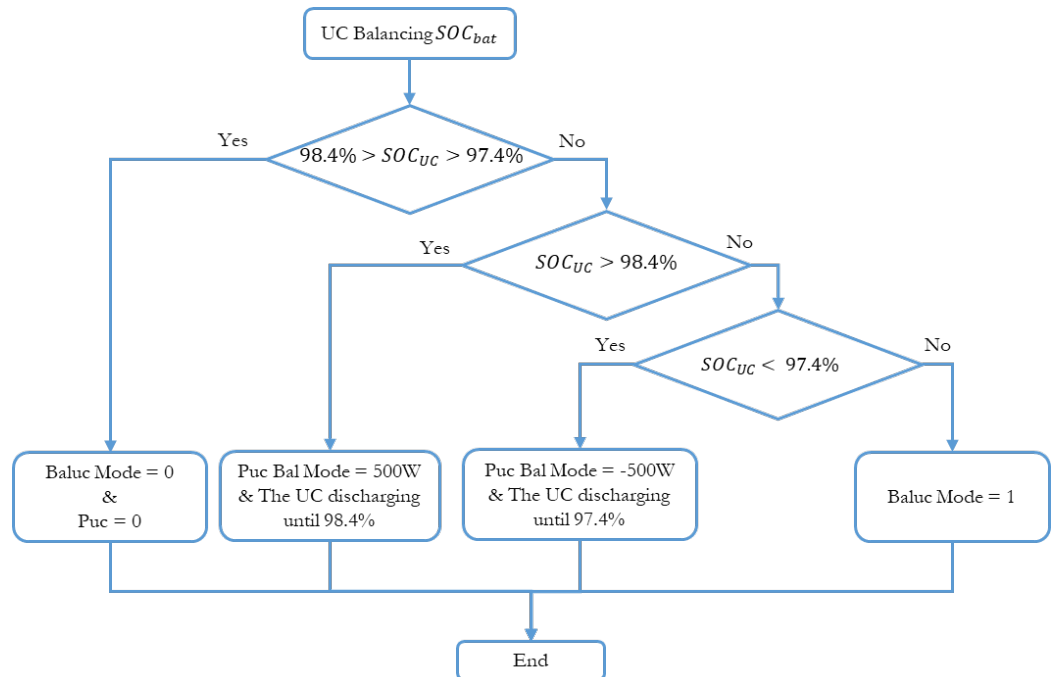Puc Bal Mode = -500W & The UC discharging until 97.4%

Baluc Mode = 1

End

**Figure 15.** Flowchart of ultracapacitor level balancing algorithm.

### 5.1. Diesel Engine Disconnected Mode (DEDM)

This mode is activated when battery SOC is greater than 25% ($Soc_{bat} > 25\%$). In this case, the PV generator operates either in MPPT mode or in Off-MPPT (Power Curtailment). Therefore, it has two sub-modes: power curtailment mode (PCM) and MPPT mode (MPPTM).

### 5.1.1. Power Curtailment Mode (PCM)

This operating mode is selected when the power of the photovoltaic generator meets the total load demand and the two storage elements are fully charged i.e., ($Soc_{bat} \geq 90\%$), The PV power must be limited to a reference value lower than $P_{mpp}$ (Maximum PowerPoint). The control algorithm enabling PCM is illustrated by Figure 9b.

### 5.1.2. Maximum Power Point Tracking Mode (MPPTM)

This mode is activated when the state of charge of the battery is less than the maximum permissible state (25% $\leq Soc_{bat} < 90\%$). In this case, the PV generator operates in MPPT mode to extract the maximum amount of electrical energy depending on the climate conditions. The storage elements have the possibility of absorbing or compensating to keep the DC bus around its value of reference $Vdc_{ref} = 700$ V, the diesel generator is stopped, and all loads are connected.

### 5.2. Diesel Engine Connected Mode (DECM)

This mode is selected when the state of charge of the battery pack is equal to 25%. In this case, the diesel generator operates at its nominal power in parallel with the PV in MPPT mode and charges the storage elements up to 90%.

### 5.3. First Priority Load Mode (FPLM)

When the Diesel generator is operating alone and the state of charge of the batteries and the ultracapacitor is insufficient and continues to charge (weak climatic conditions) below 10%, the system will be unable to satisfy the main load (load P1). In this case, the load must be disconnected to allow the hybrid storage device to charge.

### 5.4. Second Priority Load Mode (SPLM)

If the state of charge of the hybrid storage is between 10% and 15% ($10\% \leq Soc_{bat} < 15\%$), the load with the second priority (load P2) will be disconnected and only the load with the priority (load P1) will remain connected.

### 5.5. Third Priority Load Mode (TPLM)

This mode is activated when the operation of the diesel generator is connected and when the state of charge of the batteries is below 25% but remains above 15%. To avoid an additional discharge of the batteries, the supervision algorithm will disconnect the load with the lowest priority (P3).

## 6. Results and Discussion

To validate the proposed power management strategy, the following system and mode parameters are adopted: Table 3 provides parameters of PV generator and Table 4 summarizes DC system parameters. AC source parameters are given in Table 5. The controller parameters for both grid-connected and off-grid modes of the hybrid power system are provided in Table 6. The solar irradiance profile is shown by Figure 16.

**Table 3.** PV generator parameters.

| PV Generator Reference | DC Converter |
|---|---|
| BPSolar SX3190 | $L_{pv}$: 5 mH |
| $N_s$: 16, $N_p$: 6 | $C_{pv}$: 5 µF |
| $P_n$: 260.43 | |

**Table 4.** DC system parameters.

| Lead-Acid Battery | DC Converter | Ultracapacitor | DC Converter | DC Bus |
|---|---|---|---|---|
| 250 V, 40 Ah, $\tau_{bat}$ = 1.5 s | $L_{bat}$ = 4 mH | 5 F, $R_{uc}$ = 8.9 mΩ, $V_{uc}$ = 215 V | $L_{uc}$ = 5 mH | $Vdc_{ref}$ = 700 V, $C_{bus}$ = 2 mF |

**Table 5.** AC source parameters.

| Diesel Engine Parameters | Filter Parameters |
|---|---|
| $P_n$= 20 kW, $w_n$ = 1500 rpm, $\tau_1$ = 0.01 s, $\tau_2$ = 0.02 s, K = 40, Torque limits [0 1.1] | $R_f$ = 2.66 Ω, $L_f$ = 47 mH, $C_f$ = 100 µF, $T_s$ = 5 $\times 10^{-5}$, $f_s$ = 5 kHz |

**Table 6.** Connection mode control parameters.

| Disconnected Mode | Connected Mode |
|---|---|
| PLL: $K_p$ = 0.2325, $K_i$ = 5.254 | PLL: $K_p$ = 0.1114, $K_i$ = 3.3416 |
| Filter: $K_p$ = 1.200, $K_i$ = 300.251 | Filter: $K_p$ = 1.1000, $K_i$ = 136.7273 |

DC bus voltage, as shown in Figure 17, is clearly following its reference (700 V). For regulation of the DC bus voltage $Vdc$, the inverter intervenes by absorbing the surplus current to inject it into the storage sources and discharge the ultracapacitor until $Vdc$ = 700 V. In steady-state, the voltage across the DC bus remains constant due to fast dynamic voltage regulator that maintains it at its reference value ($Vdc_{ref}$ = 700 V). Few disturbances have been observed in DC bus voltage at $t$ = 10 s, 20 s, and 25 s with change in operating modes, which are happened due to sudden changes in PV power generation and load requirements.

Figures 18 and 19 show the DC power and current outputs of PV generator, battery storage, and ultracapacitor following proposed power management strategy under sudden changes in irradiance and load profiles. The ultracapacitor is rapidly balancing power demand mismatch at balancing at $t$ = 10 s, 20 s, and 25 s. It should be noted that the DC sources quickly meet system requirements in terms of power demand in both DC and AC buses. Different operating modes of the system start with the MPPT mode at 0.10 s.
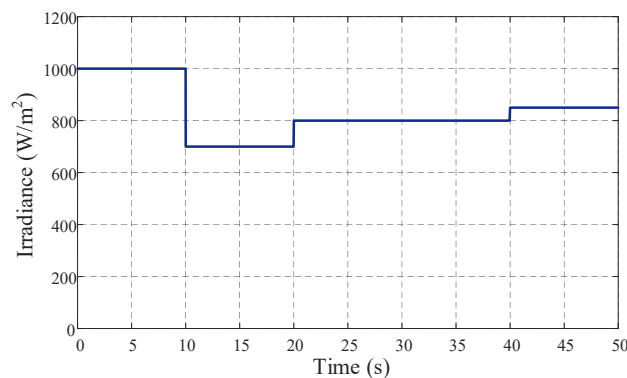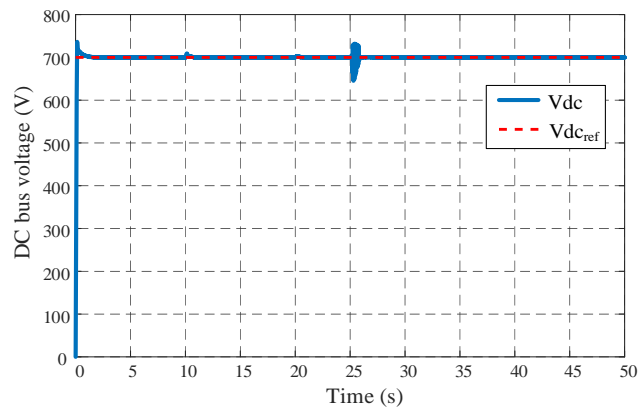


**Figure 16.** Irradiance profile.

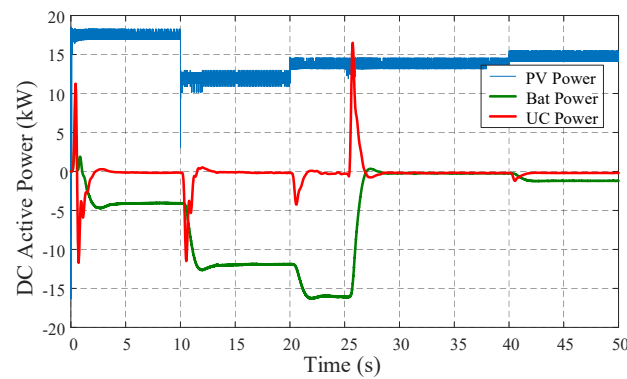**Figure 17.** DC bus voltage.



**Figure 18.** Power output profiles: PV (blue), battery (green), and ultracapacitor (red).
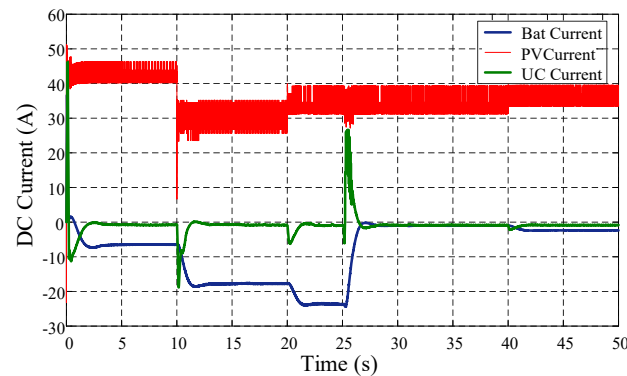


**Figure 19.** Current profiles: PV (red), battery (blue), and ultracapacitor (green).

When $P_{PV} > P_{Load}$, PV generator supplies the required power to load and the power surplus will be stored in both battery and ultracapacitor.

With low PV power output and increase in load demand ($G$ = 700 W/m$^2$, $P$ = 25 kW), DG intervenes and the DECM mode is activated at $t$ = 10 s to ensure continuous power supply to the load while also charging the battery. At instant $t$ = 25 s, the storage system is sufficiently charged and the requested load demand is satisfied which leads to the switch to the PCM mode. DG is also disconnected from the hybrid power system, as combination of PV and hybrid storage systems are enough to meet the load demand. At instant $t$ = 40 s and after a slight disturbance, the MPPT mode is activated again and the battery begins recharging. Figures 20 and 21 present the current profiles of load and DG, respectively. Load is increased between $t$ = 10 s to 25 s, DG connects to the system to meet the load demand during this period because DC power generation and storage systems are unable to meet this increasing demand.

Figure 22 illustrates the two operating modes of DG disconnection and connection with the system. The specified mode appears between $t$ = 10 s and 25 s when active power demand is requested and it cannot be met by only DC power generation and storage systems ($P_{Load} < P_{dc}$). In this case, DG connects and supplies to the load in the connected mode.

Figure 23 illustrates the case where the inverter and DG are connected with disturbances due to synchronization of the two voltage sources in the two operating modes. Due to the DG starting, voltage is provided by the inverter (disconnected mode) until $t$ =13 $s$ when the DG stabilizes.

Battery and ultracapacitor SOC levels are given in Figures 24 and 25, respectively. Initial SOC of battery is set at 60%. Hence PV generator operates in MPPT mode and the battery is continuously charging. It is charging a little faster when DG is also providing power. The ultracapacitor is also balancing real-time energy fluctuations like when DG is connected to the system and later disconnected from it.
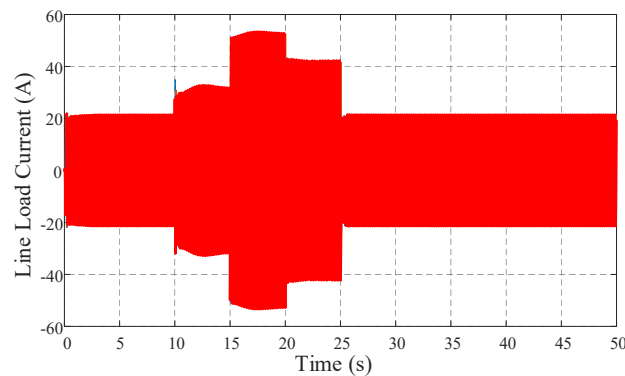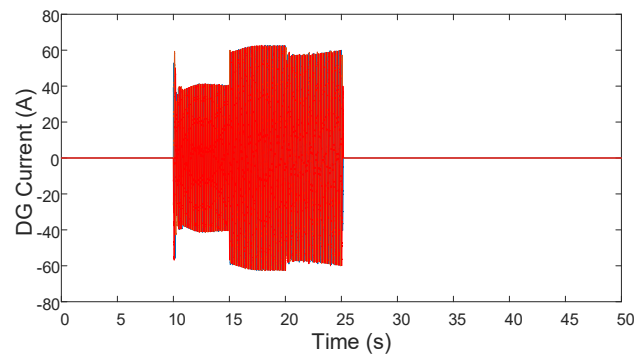
**Figure 20.** Load current.

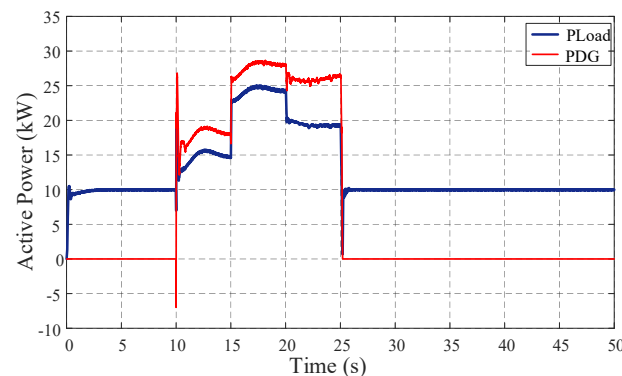**Figure 21.** Diesel generator current profile.

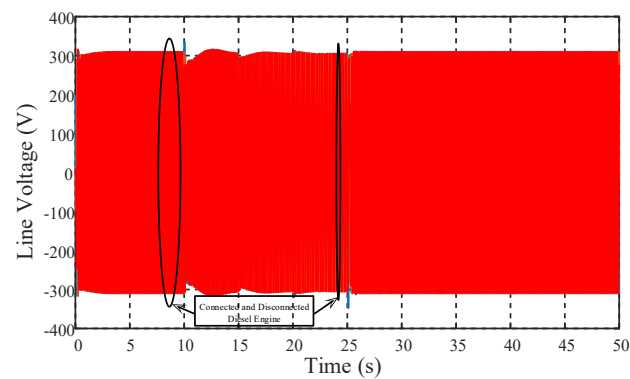**Figure 22.** Active power required by AC power load (blue), and diesel generator active power output (red).
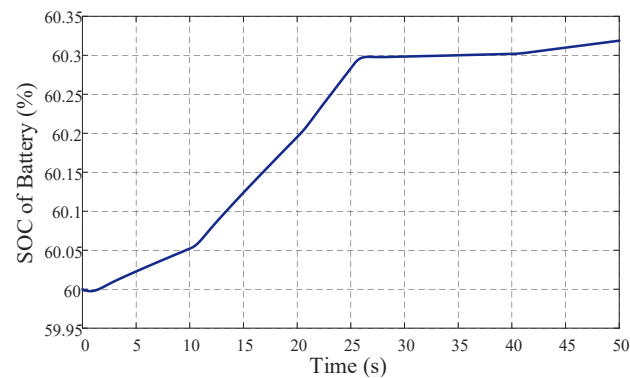
**Figure 23.** AC output voltage profile.
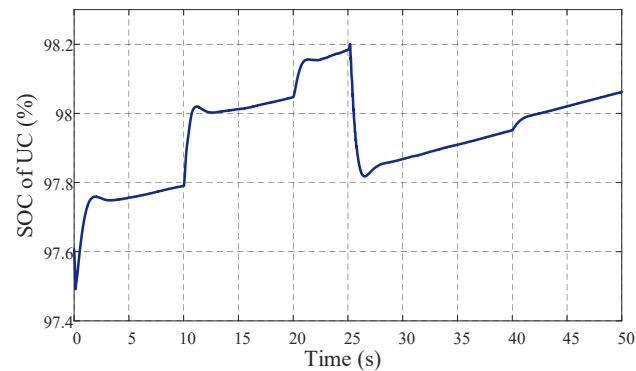


**Figure 24.** Battery SOC.



**Figure 25.** Ultracapacitor SOC.

## 7. Conclusions

In this paper, a hybrid system (PV generator–batteries–ultracapacitor and diesel generator) has been proposed for providing continuous power supply to a mobile hospital to ensure better treatment of patients in a remote area, particularly in the event of a pandemic situation such as COVID-19. In this context, an effective power management strategy was proposed to improve the hybrid power system supplying efficiency and optimizing energy consumption. The DC bus of the hybrid system is controlled by a battery and an ultracapacitor. The AC bus is controlled using two different methods: dq-frame and voltage oriented control, and their selection is determined based on the grid connectivity. The DC bus was regulated using a frequency separation controller, in which both battery and ultracapacitor can operate in charging and discharging modes. The AC bus dq-frame and voltage-oriented-based controls have proven their effectiveness in terms of dynamic power management to meet load requirements of shelter hospital.

## References

1.  Ouma, P.O.; Maina, J.; Thuranira, P.N.; Macharia, P.M.; Alegana, V.A.; English, M.; Okiro, E.A.; Snow, R.W. Access to emergency hospital care provided by the public sector in sub-Saharan Africa in 2015: A geocoded inventory and spatial analysis. *Lancet Glob. Health* **2018**, *6*, 342–350. [CrossRef]
2.  Juran, S.; Broer, P.N.; Klug, S.J.; Snow, R.C.; Okiro, E.A.; Ouma, P.O.; Snow, R.W.; Tatem, A.J.; Meara, J.G.; Alegana, V.A. Geospatial mapping of access to timely essential surgery in sub-Saharan Africa. *BMJ Glob. Health* **2018**, *3*, e000875. [CrossRef] [PubMed]
3.  Bakowski, J. A mobile hospital–its advantages and functional limitations. *Int. J. Saf. Secur. Eng.* **2016**, *6*, 746–754. [CrossRef]
4.  Issa, M.; Ibrahim, H.; Hosni, H.; Ilinca, A.; Rezkallah, M. Effects of Low Charge and Environmental Conditions on Diesel Generators Operation. *Eng* **2020**, *1*, 137–152. [CrossRef]
5.  Raghuwanshi, S.S.; Arya, R. Reliability evaluation of stand-alone hybrid photovoltaic energy system for rural healthcare centre. *Sustain. Energy Technol. Assess.* **2020**, *37*, 100624. [CrossRef]
6.  Aussel, D.; Neveu, P.; Tsuanyo, D.; Azouamh, Y. On the equivalence and comparison of economic criteria for energy projects: Application on PV/diesel hybrid system optimal design. *Energy Convers. Manag.* **2018**, *163*, 493–506. [CrossRef]
7.  Zia, M.F.; Elbouchikhi, E.; Benbouzid, M. An energy management system for hybrid energy sources-based stand-alone marine microgrid. In *IOP Conference Series: Earth and Environmental Science*; IOP Publishing: Bristol, UK, 2019; Volume 322, p. 012001.
8.  Sabihuddin, S.; Kiprakis, A.E.; Mueller, M. A numerical and graphical review of energy storage technologies. *Energies* **2015**, *8*, 172–216. [CrossRef]
9.  Haidl, P.; Buchroithner, A.; Schweighofer, B.; Bader, M.; Wegleiter, H. Lifetime analysis of energy storage systems for sustainable transportation. *Sustainability* **2019**, *11*, 6731. [CrossRef]
10. Agbli, K.S.; Hilairet, M.; Gustin, F. Real-Time Control Based on a CAN-Bus of Hybrid Electrical Systems. *Energies* **2020**, *13*, 4502. [CrossRef]
11. González, A.G.; García-Sanz-Calcedo, J.; Salgado, D.R. A quantitative analysis of final energy consumption in hospitals in Spain. *Sustain. Cities Soc.* **2018**, *36*, 169–175. [CrossRef]
12. Mohamed, M.A.; Eltamaly, A.M.; Alolah, A.I. Sizing and techno-economic analysis of stand-alone hybrid photovoltaic/wind/diesel/battery power generation systems. *J. Renew. Sustain. Energy* **2015**, *7*, 063128. [CrossRef]
13. Islam, S.M.; Nayar, C.V.; Abu-Siada, A.; Hasan, M.M. Power Electronics for Renewable Energy Sources. In *Power Electronics Handbook*; Elsevier: Amsterdam, The Netherlands, 2018; pp. 783–827.
14. Lagrange, A.; de Simón-Martín, M.; González-Martínez, A.; Bracco, S.; Rosales-Asensio, E. Sustainable microgrids with energy storage as a means to increase power resilience in critical facilities: An application to a hospital. *Int. J. Electr. Power Energy Syst.* **2020**, *119*, 105865. [CrossRef]
15. Alonso, J.B.; Sandwell, P.; Nelson, J. The potential for solar-diesel hybrid mini-grids in refugee camps: A case study of Nyabiheke camp, Rwanda. *Sustain. Energy Technol. Assess.* **2021**, *44*, 101095.
16. Jahangir, M.H.; Cheraghi, R. Economic and environmental assessment of solar-wind-biomass hybrid renewable energy system supplying rural settlement load. *Sustain. Energy Technol. Assess.* **2020**, *42*, 100895. [CrossRef]
17. Elia, S.; Santantonio, A. Fire risk in MTBF evaluation for UPS system. *Adv. Electr. Electron. Eng.* **2016**, *14*, 189–195. [CrossRef]
18. Elia, S.; Santini, E.; Tobia, M. Comparison between different electrical configurations of emergency diesel generators for redundancy and reliability improving. *Period. Polytech. Electr. Eng. Comput. Sci.* **2018**, *62*, 144–148. [CrossRef]
19. Boccaletti, C.; Elia, S.; Salas M, E.; Pasquali, M. High reliability storage systems for genset cranking. *J. Energy Storage* **2020**, *29*, 101336. [CrossRef]
20. Mutarraf, M.U.; Terriche, Y.; Niazi, K.A.K.; Khan, F.; Vasquez, J.C.; Guerrero, J.M. Control of hybrid diesel/PV/battery/ultra-capacitor systems for future shipboard microgrids. *Energies* **2019**, *12*, 3460. [CrossRef]
21. Tah, A.; Das, D. Operation of small hybrid autonomous power generation system in isolated, interconnected and grid connected modes. *Sustain. Energy Technol. Assess.* **2016**, *17*, 11–25. [CrossRef]
22. Yin, C.; Wu, H.; Locment, F.; Sechilariu, M. Energy management of DC microgrid based on photovoltaic combined with diesel generator and supercapacitor. *Energy Convers. Manag.* **2017**, *132*, 14–27. [CrossRef]
23. Gassab, S.; Radjeai, H.; Mekhilef, S.; Choudar, A. Power management and coordinated control of standalone active PV generator for isolated agriculture area-case study in the South of Algeria. *J. Renew. Sustain. Energy* **2019**, *11*, 015305. [CrossRef]

24. Kim, Y.S.; Kim, E.S.; Moon, S.I. Frequency and voltage control strategy of standalone microgrids with high penetration of intermittent renewable generation systems. *IEEE Trans. Power Syst.* **2015**, *31*, 718–728. [CrossRef]

25. Choudar, A.; Boukhetala, D.; Barkat, S.; Brucker, J.M. A local energy management of a hybrid PV-storage based distributed generation for microgrids. *Energy Convers. Manag.* **2015**, *90*, 21–33. [CrossRef]

26. Wen, S.; Wang, S.; Liu, G.; Liu, R. Energy management and coordinated control strategy of PV/HESS AC microgrid during islanded operation. *IEEE Access* **2018**, *7*, 4432–4441. [CrossRef]

27. Klugmann-Radziemska, E.; Ostrowski, P. Chemical treatment of crystalline silicon solar cells as a method of recovering pure silicon from photovoltaic modules. *Renew. Energy* **2010**, *35*, 1751–1759. [CrossRef]

28. Huang, W.H.; Shin, W.J.; Wang, L.; Sun, W.C.; Tao, M. Strategy and technology to recycle wafer-silicon solar modules. *Sol. Energy* **2017**, *144*, 22–31. [CrossRef]

29. Nayak, P.K.; Mahesh, S.; Snaith, H.J.; Cahen, D. Photovoltaic solar cell technologies: Analysing the state of the art. *Nat. Rev. Mater.* **2019**, *4*, 269–285. [CrossRef]

30. Tang, K.H.; Chao, K.H.; Chao, Y.W.; Chen, J.P. Design and implementation of a simulator for photovoltaic modules. *Int. J. Photoenergy* **2012**, *2012*, 368931. [CrossRef]

31. Widyolar, B.; Jiang, L.; Brinkley, J.; Hota, S.K.; Ferry, J.; Diaz, G.; Winston, R. Experimental performance of an ultra-low-cost solar photovoltaic-thermal (PVT) collector using aluminum minichannels and nonimaging optics. *Appl. Energy* **2020**, *268*, 114894. [CrossRef]

32. Sarita, K.; Devarapalli, R.; Rai, P. Modeling and control of dynamic battery storage system used in hybrid grid. *Energy Storage* **2020**, *2*, e146. [CrossRef]

33. Li, Y.; Vilathgamuwa, M.; Farrell, T.; Tran, N.T.; Teague, J. A physics-based distributed-parameter equivalent circuit model for lithium-ion batteries. *Electrochim. Acta* **2019**, *299*, 451–469. [CrossRef]

34. Tran, M.K.; DaCosta, A.; Mevawalla, A.; Panchal, S.; Fowler, M. Comparative study of equivalent circuit models performance in four common lithium-ion batteries: LFP, NMC, LMO, NCA. *Batteries* **2021**, *7*, 51. [CrossRef]

35. Tran, M.K.; Mathew, M.; Janhunen, S.; Panchal, S.; Raahemifar, K.; Fraser, R.; Fowler, M. A comprehensive equivalent circuit model for lithium-ion batteries, incorporating the effects of state of health, state of charge, and temperature on model parameters. *J. Energy Storage* **2021**, *43*, 103252. [CrossRef]

36. Logerais, P.O.; Camara, M.; Riou, O.; Djellad, A.; Omeiri, A.; Delaleux, F.; Durastanti, J. Modeling of a supercapacitor with a multibranch circuit. *Int. J. Hydrogen Energy* **2015**, *40*, 13725–13736. [CrossRef]

37. Helseth, L.E. Modelling supercapacitors using a dynamic equivalent circuit with a distribution of relaxation times. *J. Energy Storage* **2019**, *25*, 100912. [CrossRef]

38. Sakamoto, O. An example of a diesel generator model with fluctuating engine torque for transient analysis using XTAP. *J. Int. Counc. Electr. Eng.* **2016**, *6*, 31–35. [CrossRef]

39. Mishra, S.; Ramasubramanian, D. Improving the small signal stability of a PV-DE-dynamic load-based microgrid using an auxiliary signal in the PV control loop. *IEEE Trans. Power Syst.* **2014**, *30*, 166–176. [CrossRef]

40. Christopher, I.W.; Ramesh, R. Comparative study of P&O and InC MPPT algorithms. *Am. J. Eng. Res. (AJER)* **2013**, *2*, 402–408.

41. Carrasco, J.A.; de Quirós, F.G.; Alavés, H.; Navalón, M. An analog maximum power point tracker with pulsewidth modulator multiplication for a solar array regulator. *IEEE Trans. Power Electron.* **2018**, *34*, 8808–8815. [CrossRef]

42. Bhattacharyya, S.; Samanta, S.; Mishra, S. Steady Output and Fast Tracking MPPT (SOFT-MPPT) for P&O and InC Algorithms. *IEEE Trans. Sustain. Energy* **2020**, *12*, 293–302.

43. Tao, Y.; Liu, Q.; Deng, Y.; Liu, X.; He, X. Analysis and mitigation of inverter output impedance impacts for distributed energy resource interface. *IEEE Trans. Power Electron.* **2014**, *30*, 3563–3576. [CrossRef]

44. Ramezani, M.; Li, S.; Sun, Y. DQ-reference-frame based impedance and power control design of islanded parallel voltage source converters for integration of distributed energy resources. *Electr. Power Syst. Res.* **2019**, *168*, 67–80. [CrossRef]

45. Kosari, M.; Hosseinian, S.H. Decentralized reactive power sharing and frequency restoration in islanded microgrid. *IEEE Trans. Power Syst.* **2016**, *32*, 2901–2912. [CrossRef]

46. Mazhar-Ul-Haq, S.; Ram, S.; Subramanyam, J. Voltage Oriented Control (VOC) Of The PWM Rectifier Using Active Filtering Function. *Int. J. Eng. Technol.* **2018**, *7*, 90–93. [CrossRef]

47. Zamani, M.H.; Riahy, G.H.; Abedi, M. Rotor-speed stability improvement of dual stator-winding induction generator-based wind farms by control-windings voltage oriented control. *IEEE Trans. Power Electron.* **2015**, *31*, 5538–5546. [CrossRef]